Kinetics and Catalysis, Vol. 43, No. 2, 2002, pp. 233–244. Translated from Kinetika i Kataliz, Vol. 43, No. 2, 2002, pp. 256–268.

Periodic, Mixed-Mode, and Chaotic Regimes in the Belousov–Zhabotinskii Reaction Catalyzed by Ferroin

E. Yu. Kalishin, M. M. Goncharenko, V. A. Khavrus', and P. E. Strizhak

Pisarzhevskii Institute of Physical Chemistry, National Academy of Sciences of Ukraine, Kiev, Ukraine

Received June 16, 2001

Abstract—The periodic, mixed-mode, and chaotic regimes in the ferroin-catalyzed Belousov–Zhabotinskii (BZ) reaction observed in a continuous stirred tank reactor (CSTR) reactor at various flow rates were experimentally studied. It was found that an increase in the flow rate resulted in the appearance of various complex oscillations. The possibility of the numerical simulation of experimentally observed asymptotic mixed-mode oscillations and chaotic regimes with the use of a kinetic scheme that includes experimental rate constants of each step of the ferroin-catalyzed BZ reaction was first demonstrated. The reaction scheme adequately describes the bifurcation sequence of experimentally observed oscillating regimes.

INTRODUCTION

The Belousov–Zhabotinskii (BZ) reaction (the catalytic oxidation of malonic acid (MA) by bromate ions in an acid medium) is the best studied reaction among chemical autooscillation systems [1–5]. Cerium compounds or ferroin (tris(1,10-phenanthroline)iron(II)) are the most frequently used catalysts of this reaction [1, 4, 5]. The BZ reaction catalyzed by cerium ions was studied in detail [6–9]. Various kinetic schemes were proposed for this reaction to describe experimentally observed regimes [8, 10–15]. In particular, a study of the kinetics of individual steps of the BZ reaction resulted in a kinetic scheme of 80 reactions [10]. The ferroin-catalyzed BZ reaction is less understood, although it is used to study nonlinear phenomena in spatially distributed systems [5, 16, 17], to develop new analytical methods for the determination of trace metal ions [18, 19], and to analyze the state of ecological systems [20]. Note that various periodic, mixed, and chaotic regimes were observed in the BZ reaction catalyzed by either cerium ions or ferroin [1, 6, 7, 9, 14]. However, until now no kinetic scheme of the BZ reaction (with the use of experimental rate constants of individual reaction steps) for describing these complex regimes [10–14, 21, 22] has been established. Györgyi and Field [11] found that mixed and chaotic regimes observed in the BZ reaction catalyzed by cerium(III) ions can be described only by varying the rate constants of certain steps by several orders of magnitude. Previously [23], a kinetic scheme of the ferroin-catalyzed BZ reaction was proposed based on an analysis of published data. The experimentally measured rate constants of individual reaction steps were used in this scheme. An analysis of this kinetic scheme demonstrated that it describes the simplest transient mixed-mode oscillations observed in experiments.

This work was devoted to an experimental study of various periodic, mixed, and chaotic regimes in the ferroin-catalyzed BZ reaction performed in a continuous-stirred tank reactor (CSTR). The aim of this study was also to describe the experimentally observed asymptotic mixed and chaotic regimes with the use of the experimental rate constants of each step of the BZ reaction based on a numerical simulation with the use of the kinetic scheme proposed previously for the ferroin-catalyzed BZ reaction.

EXPERIMENTAL

The experiments were performed in a 14.8-ml CSTR thermostatted at 295.5 K. The reactants were supplied to the reactor in the following concentrations: $[H_2SO_4]_0 = 0.32$ M, $[MK]_0 = 0.16$ M, $[KBrO_3]_0 = 0.19$ M, and $[\text{ferroin}]_0 = 0.0017$ M. The reaction mixture was stirred with an electromechanical stirrer at a constant rate of 900 rpm. The reactants were supplied with a precalibrated hydrostatic pump, whose outflow rate depends on the height of a solution over the reactor level. In the experiments, the flow rate (k_0, s^{-1}) was varied at a constant step of 1.7×10^{-4} s^{-1}. In this work, the value of k_0 rather than its inverse, which corresponds to the contact time, was used because the flow rate was chosen as the control parameter in the literature devoted to the bifurcations of autooscillation regimes of the BZ reaction in a CSTR. We did not observe a hysteresis phenomenon on increasing or decreasing k_0 in the experiments. The course of the reaction was monitored by measuring the potential of a platinum point electrode in time, referenced to a silver–silver chloride electrode, which was connected to a reactor solution through a salt bridge. The time dependence of the platinum point electrode potential corresponding to an asymptotic oscillation regime was recorded after a transient stage (no shorter than 1500 s). The analog signals

0023-1584/02/4302-0233$27.00 © 2002 MAIK "Nauka / Interperiodica"

were converted into digital signals by an analog-to-digital converter at 0.1-s intervals and stored on a computer.

The quantitative characteristics (period and amplitude) of the experimental autooscillation regimes were found with the use of programs developed for an IBM-compatible personal computer. The maximum Lyapunov exponent (MLE), which characterizes the degree of chaos of the resulting time series, was calculated according to a published algorithm [24] at the dimensionality of a reconstructed phase space equal to 4. The rate equations written in accordance with the proposed kinetic scheme were numerically simulated using the LSODE integration package [25].

RESULTS AND DISCUSSION

Figure 1 presents typical mixed-mode oscillations [9, 14, 15] observed at different flow rates. These oscillations are alternating sequences of large- and small-amplitude excursions. Let us denote the large-amplitude oscillations with an amplitude of the platinum point electrode potential higher than 0.08 V by L and the small-amplitude oscillations with an amplitude smaller than 0.05 V by S. Superscripted figures by the symbols L and S indicate the numbers of repeated successive excursions of the same type. Figure 1a demonstrates the simplest mixed-mode oscillations of the L_1S_1 type. Asymptotic oscillations of this type occur in a range of $k_0 = (3.33–3.83) \times 10^{-3}$ s^{-1}. Figure 1b demonstrates a more complex periodic regime of the $(L_1S_3)(L_1S_4)$ type, which is a sequential alternation of (L_1S_3)- and (L_1S_4)-type oscillations, observed in the range $k_0 = (5.17–5.33) \times 10^{-3}$ s^{-1}. We found the occurrence of chaotic regimes at high flow rates. In particular, at $k_0 = 10.33 \times 10^{-3}$ s^{-1}, a chaotic regime was observed, which consisted of a well-defined large-amplitude peak and subsequent small-amplitude oscillations (Fig. 1c). Henceforth, we will denote this type of oscillation by C_L. The nonrepeated random structure of the reconstructed phase portrait is indicative of a chaotic character of the observed regime (Fig. 2). The other evidence for the chaotic character of the observed aperiodic autooscillations is a positive MLE value, which is equal to 0.111 s^{-1}. In the range $k_0 = (11.33–14.33) \times 10^{-3}$ s^{-1}, quasi-periodic (**QP**) oscillations were detected, which are small-amplitude oscillations with a periodically changed amplitude (Fig. 1d).

To determine the bifurcation sequence of mixed-mode oscillations at different flow rates, we performed a detailed study of asymptotic regimes observed at different values of k_0. Table 1 summarizes the types of asymptotic mixed modes observed at flow rates higher than $k_0 = 0.5 \times 10^{-3}$ s^{-1}. Lower flow rates are much more difficult to use because of a long transient regime, which is longer than several tens of hours. At $k_0 = 0.5 \times 10^{-3}$ s^{-1}, periodic large-amplitude R-oscillations were observed, which did not disappear upon the continuous supply of the reactants for 20 h. At $k_0 = 2.83 \times 10^{-3}$ s^{-1}, L_7S_1 oscillations were observed, in which one small-amplitude excursion was observed after seven large-amplitude excursions. At $k_0 = (3.00–3.17) \times 10^{-3}$ s^{-1}, L_5S_1 oscillations were detected in the system, whereas the simplest L_1S_1 mixed-mode oscillations were observed in the range $k_0 = (3.33–3.83) \times 10^{-3}$ s^{-1} (see Table 1 and Fig. 1a). A further increase in k_0 resulted in the appearance of the $(L_1S_1)(L_1S_2)$ oscillations, which evolved to the L_1S_2 regime at $k_0 = 4.33 \times 10^{-3}$ s^{-1}.

An analysis of data given in Table 1 indicates that the fraction of small-amplitude oscillations gradually increased as the flow rate was increased. In the general case, transitions between simple mixed-regime oscillations of the L_1S_n and L_1S_{n+1} types, which were observed in the range $k_0 = (3.33–7.50) \times 10^{-3}$ s^{-1}, occurred through a bifurcation of the addition of one S-oscillation in the sequences of L_1S_n oscillations [14, 15]. This resulted in the appearance of regimes consisting of L_1S_n and L_1S_{n+1} oscillations, as supported by the entire set of data given in Table 1. For example, on going from periodic oscillations of the L_1S_2 type to L_1S_3 oscillations at $k_0 = 4.50 \times 10^{-3}$ s^{-1}, the $2(L_1S_2)(L_1S_3)$ regime was observed, which gave way to the $(L_1S_2)(L_1S_3)$ regime at $k_0 = 4.67 \times 10^{-3}$ s^{-1}. The bifurcations of the L_1S_3, L_1S_4, L_1S_5, L_1S_7, and L_1S_9 regimes occurred in a similar manner (see Table 1 and Fig. 1b). The L_1S_9 regime is the most complex periodic regime detected in our experiments. More complex regimes were observed in the range $k_0 = (7.67–11.17) \times 10^{-3}$ s^{-1} as chaotic mixtures of L_1S_n oscillations, in which the number of small-amplitude excursions irregularly changed (see Table 1 and Fig. 1c). Note that the maximum Lyapunov exponents (Table 2), which take positive values, suggest that chaotic rather than periodic regimes occurred in the above range of k_0. At $k_0 = 11.33 \times 10^{-3}$ s^{-1}, large-amplitude L-oscillations disappeared from chaotic sequences, and only quasi-periodic oscillations, whose amplitude was changed periodically, were observed (see Table 1 and Fig. 1d). Oscillations of this type occurred in a range of $k_0 = (11.33–14.33) \times 10^{-3}$ s^{-1}. At the flow rate $k_0 > 14.33 \times 10^{-3}$ s^{-1}, a steady state (**SS**) was observed in the system.

To simulate the experimentally observed mixed-mode oscillations, we used the previously proposed kinetic scheme [23], which is given in Table 3. This kinetic scheme consists of 29 reactions for 12 chemical compounds, whose concentrations are independent variables. This scheme may be tentatively subdivided into the following three groups of reactions: (A) reactions between bromine-containing compounds, (B) reactions with the participation of bromine-containing compounds and MA derivatives, and (C) reactions with the participation of ferroin. Group A reactions are common for all bromate oscillators [1], and they include the

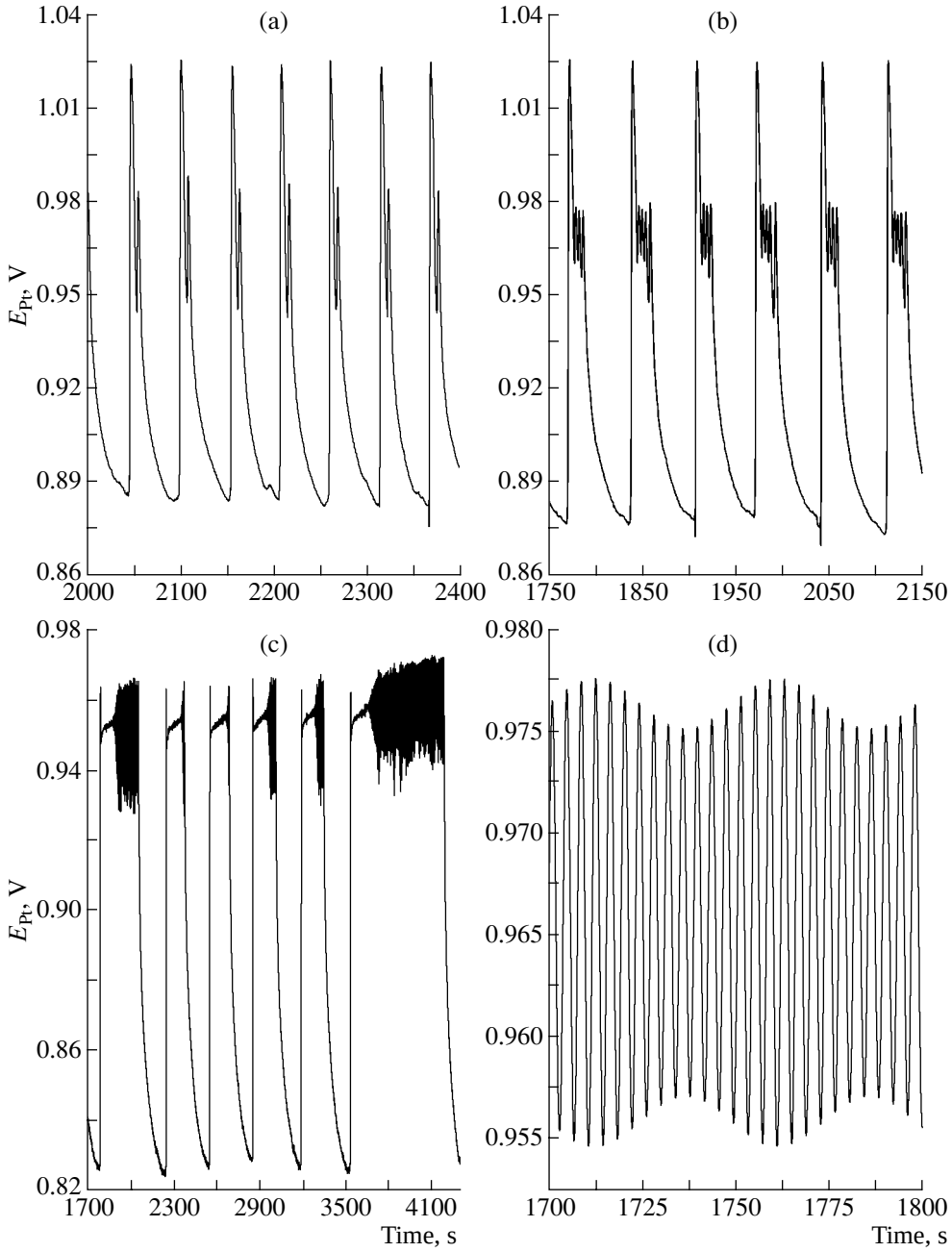

Fig. 1. Time dependence of the platinum point electrode potential in the BZ reaction at the flow rates k_0, s^{-1}: (a) 3.50×10^{-3} (L_1S_1 oscillations), (b) 5.33×10^{-3} ((L_1S_3)(L_1S_4) oscillations), (c) 10.33×10^{-3} (large-amplitude chaotic C_L oscillations), and (d) 13.33×10^{-3} (quasi-periodic QP oscillations).

reactions of bromate ions and their reduction products. Group B reactions describe the oxidation of MA and its derivatives except for reactions with the participation of the catalyst. Group C reactions describe the interactions of ferroin (Fe^{2+}), ferroin (Fe^{3+}), and other components of the autooscillation reaction.

In accordance with the kinetic scheme given in Table 3, the rate equations are briefly written as follows:

$$\frac{dC_i}{dt} = f_i(C_1, \ldots, C_i, \ldots, C_{12}) + k_0(C_i^0 - C_i), \quad i = 1, 2, \ldots, 12, \tag{1}$$

where C_i is the concentration of the ith component in the reactor, C_i^0 is its concentration at the reactor inlet, k_0 is the flow rate, and $f_i(C_1, \ldots C_i, \ldots C_{12})$ is the rate of change of the ith component concentration written in

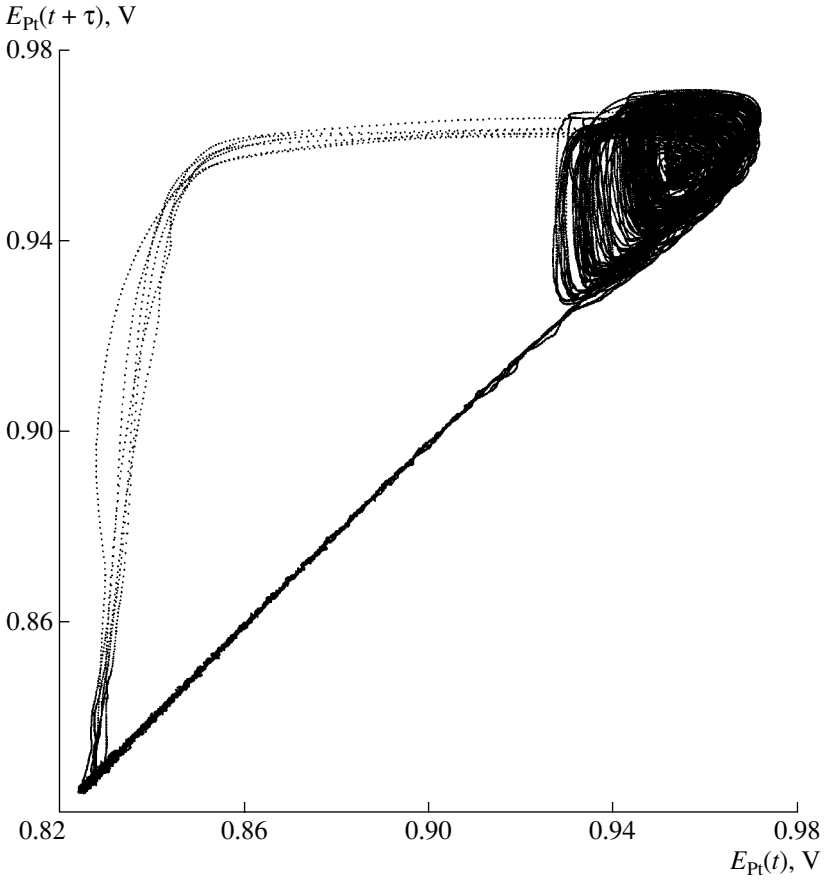

Fig. 2. Phase portrait reconstructed for a chaotic trajectory shown in Fig. 1c. The time delay τ is 1 s.

accordance with the kinetic scheme presented in Table 3. The system of differential Eqs. (1) is given in the Appendix. The calculation was performed at $T = 298$ K and the following inlet and initial reactant concentrations: $[Br^-]_0 = 10^{-7}$ M, $[MK]_0 = 0.22$ M, $[BrO_3^-]_0 = 0.15$ M, and $[\text{ferroin}]_0 = 0.0017$ M. The flow rate k_0 was chosen as the control parameter. To construct a bifurcation diagram of autooscillation regimes at given values of the control parameters, the system of differential Eqs. (1) was integrated; as a result, kinetic curves were obtained. To exclude transient regimes from consideration, the first 10000 s were not taken into account. Oscillation amplitudes were determined by analyzing the obtained kinetic curves, and these values were plotted in a bifurcation diagram at a given value of k_0. At the same value of k_0, the concentrations of different components of the test system changed with time in qualitatively different manners. The widest variety of oscillation regimes was found for HOBr. Therefore, Figs. 3 and 4 illustrate autooscillation regimes and bifurcation diagrams, respectively, by the example of HOBr. Note that the time dependence of the concentration of hypobromous acid is inconsistent with the experimental dependence of the platinum point electrode potential, because the potential and the oscillation phase of a platinum point electrode depend on the actual concentrations of all components of the autooscillation system. However, such a comparison can be made for experimental and numerically simulated bifurcations of autooscillation regimes. Tables 4 and 5 summarize the autooscillation regimes and bifurcation points found by numerical simulation.

Data given in Fig. 3 illustrate various oscillation regimes obtained by numerical simulation. Figure 3a demonstrates the LSJ regime, which is a repeated sequence of large-amplitude L-oscillations, small-amplitude S-oscillations, and oscillations as concentration jumps denoted by J. Unfortunately, we failed to experimentally observe J-oscillations by detection using platinum point, bromide, glass, and carbon electrodes. Small-amplitude oscillations disappeared as the flow rate was increased. Because of this, the LJ regime (Fig. 3b) was observed, which was transformed into the L_1S_1 regime when k_0 was further increased (Fig. 3c). This regime only qualitatively corresponds to that found experimentally (see Fig. 1a) because S-oscillations obtained in the numerical simulation manifest themselves as a wave near a minimum concentration of hypobromous acid. Periodic complex-shaped oscillations, which we designated as regular (R), were

observed when k_0 was further increased. Figure 3d shows an example of R-oscillations. An increase of the flow rate resulted in the addition of small-amplitude excursions to mixed-mode oscillations. Thus, Fig. 3e demonstrates the $L_1S_3L_1S_4$ regime observed at $\log k_0$, [s^{-1}] = –1.66. This regime is consistent with that found experimentally (see Fig. 1b). The regimes shown in Figs. 3a–3e are periodic. Along with periodic oscillations, we detected chaotic C_L oscillations, which are analogous to experimentally observed oscillations, shown in Fig. 3f. The chaotic character of oscillations was supported by positive MLE values. In particular, MLE = 0.019 s^{-1} for data shown in Fig. 3f. Moreover, the phase portrait of chaotic oscillations exhibits a nonrepeated random structure, which is similar to that in Fig. 2. Note that the average time interval between large-amplitude oscillations is one order of magnitude longer than the corresponding value for the oscillations of the platinum point electrode potential (see Fig. 1c). Figure 3g demonstrates quasi-periodic oscillations (QP), which appear because of the superposition of two independent frequencies resulting in a periodic change in the amplitude of oscillations. These oscillations are consistent with those found in experiments (see Fig. 1d); however, their modulation periods differ by more than one order of magnitude. Figure 3h demonstrates periodic small-amplitude oscillations observed near the point of a steady-state stability loss, which are designated by εR.

Figure 4a demonstrates a bifurcation diagram that describes changes in the oscillation amplitude with changes in the flow rate over the entire region of occurrence of oscillations. At $\log k_0$, [s^{-1}] < –4.456, a steady state was observed. Oscillations of the LSJ type appeared as k_0 was increased; Fig. 4b demonstrates the region of occurrence of these oscillations. An analysis of this bifurcation diagram and a comparison with data given in Figs. 3a and 3b indicate that the top, medium, and bottom curves correspond to L-, J-, and S-type oscillations, respectively. The zero amplitude (bottom straight line) corresponds to a steady state.

At $\log k_0$, [s^{-1}] = (–4.456)–(–4.130) (Fig. 4b), the coexistence of a steady state (SS) and autooscillations was observed: either autooscillations or a steady state were observed, depending on initial conditions. Thus, the scheme of bifurcation transitions corresponding to the appearance of R-oscillations with increasing k_0 can be written as follows: SS ⟶ LSJ ⟶ LJ ⟶ R.

A further increase in the control parameter resulted in the appearance of chaotic oscillations through a period-doubling bifurcation and transition to the region of mixed-mode oscillations, as shown in Fig. 4c. Figure 4d demonstrates a bifurcation diagram of various mixed-mode and chaotic oscillations. At small values of k_0, various mixed-mode regimes were observed, one of which is shown in Fig. 3e.

Table 1. Asymptotic mixed-mode oscillations observed at different CSTR refresh rates

$k_0 \times 10^3$, s^{-1}	Regime
0.50–2.67	R
2.83	L_7S_1
3.00, 3.17	L_5S_1
3.33–3.83	L_1S_1
4.00, 4.17	$(L_1S_1)(L_1S_2)$
4.33	L_1S_2
4.50	$2(L_1S_2)(L_1S_3)$
4.67	$(L_1S_2)(L_1S_3)$
4.83, 5.00	L_1S_3
5.17, 5.33	$(L_1S_3)(L_1S_4)$
5.50	$(L_1S_3)2(L_1S_4)$
5.67	L_1S_4
5.83	$4(L_1S_4)(L_1S_5)$
6.00–6.33	$(L_1S_4)(L_1S_5)$
6.5	$(L_1S_4)2(L_1S_5)$
6.67	L_1S_5
6.83	$(L_1S_5)(L_1S_6)$
7.00	$2(L_1S_6)(L_1S_7)$
7.17	L_1S_7
7.33	$(L_1S_7)2(L_1S_8)$
7.50	L_1S_9
7.67–11.17	C_L
11.33–14.33	QP
>14.33	SS

Table 2. Largest Lyapunov exponents for chaotic regimes observed within the range of CSTR refresh rates (7.67–11.17) × 10^3 s^{-1}

$k_0 \times 10^3$, s^{-1}	MLE, s^{-1}
8.17	0.094
8.67	0.116
9.00	0.118
9.50	0.085
9.83	0.098
10.33	0.111
11.00	0.121

Table 3. Kinetic scheme of the ferroin-catalyzed Belousov–Zhabotinskii reaction[a]

No.	Reaction	Rate constant[b]	Reference
	A. Reactions between bromine-containing compounds		
1	$Br^- + BrO_3^- + 2H^+ \longrightarrow HOBr + HBrO_2$	0.5	[10]
2	$HOBr + HBrO_2 \longrightarrow Br^- + BrO_3^- + 2H^+$	3.3	[10]
3	$HBrO_2 + Br^- + H^+ \longrightarrow 2HOBr$	1×10^6	[10]
4	$2HOBr \longrightarrow HBrO_2 + Br^- + H^+$	2×10^{-5}	[10]
5	$HOBr + Br^- + H^+ \longrightarrow Br_2 + H_2O$	1.15×10^9	[10]
6	$Br_2 + H_2O \longrightarrow HOBr + Br^- + H^+$	2	[10]
7	$2HBrO_2 \longrightarrow BrO_3^- + HOBr + H^+$	3000	[10]
8	$BrO_3^- + HOBr + H^+ \longrightarrow 2HBrO_2$	3.75×10^{-9}	[10]
9	$BrO_3^- + HBrO_2 + H^+ \longrightarrow 2BrO_2^\bullet + H_2O$	25	[22]
10	$2BrO_2^\bullet + H_2O \longrightarrow BrO_3^- + HBrO_2 + H^+$	4.2×10^7	[22]
	B. Reactions with the participation of bromine-containing compounds and malonic acid derivatives		
11	$MA + Br_2 \longrightarrow BrMA + Br^- + H^+$	28.65	[23]
12	$MA + HOBr \longrightarrow BrMA + H_2O$	8.2	[10]
13	$BrMA + HOBr \longrightarrow$ product	0.1	[10]
14	$2BrMA^\bullet + H_2O \longrightarrow BrMA + BrTTA$	1×10^8	[10]
15	$BrMA^\bullet + BrO_2^\bullet + H_2O \longrightarrow HBrO_2 + BrTTA$	5×10^9	[10]
16	$BrMA^\bullet + MA^\bullet + H_2O \longrightarrow MA + BrTTA$	1×10^9	[10]
17	$MA^\bullet + BrO_2^\bullet \longrightarrow$ product	5×10^9	[10]
18	$MA^\bullet + BrO_3^- + H^+ \longrightarrow BrO_2^\bullet +$ product	20	[10]
19	$BrTTA \longrightarrow Br^- +$ product	1	[10]
20	$BrMA^\bullet + BrO_3^\bullet + H^+ \longrightarrow BrO_2^\bullet + BrTTA$	20	[10]
	C. Reactions with the participation of the catalyst[c]		
21	$Fe^{2+} + BrO_2^\bullet + H^+ \longrightarrow Fe^{3+} + HBrO_2$	5×10^8	[22]
22	$2Fe^{2+} + BrO_3^- + 3H^+ \longrightarrow 2Fe^{3+} + HBrO_2 + H_2O$	0.1	[22]
23	$2Fe^{2+} + HBrO_2 + 2H^+ \longrightarrow 2Fe^{3+} + HOBr + H_2O$	1	[22]
24	$2Fe^{2+} + HOBr + H^+ \longrightarrow 2Fe^{3+} + Br^- + H_2O$	5×10^{-3}	[22]
25	$2Fe^{2+} + Br_2 + H^+ \longrightarrow 2Fe^{3+} + 2Br^-$	100	[22]
26	$2Fe^{3+} + 2Br^- \longrightarrow 2Fe^{2+} + Br_2 + H^+$	See note[d]	[22]
27	$Fe^{3+} + MA \longrightarrow Fe^{2+} + MA^\bullet + H^+$	1×10^{-2}	[23]
28	$Fe^{3+} + BrMA \longrightarrow Fe^{2+} + BrMA^\bullet + H^+$	20	[23]
29	$Fe^{2+} + BrMA^\bullet + H^+ \longrightarrow Fe^{3+} + BrMA$	2×10^9	[23]

Note: MA is malonic acid, BrMA is bromomalonic acid, BrTTA is 2-bromo-2-hydroxymalonic acid, Fe^{2+} is tris(1,10-phenanthroline)iron(II) ($Fe(phen)_3^{2+}$), and Fe^{3+} is tris(1,10-phenanthroline)iron(III) ($Fe(phen)_3^{3+}$).

[a] The concentrations $[H^+] = 0.5$ M and $[H_2O] = 55.56$ M are included in the rate constants; the reaction rate constants were taken at $T = 298$ K.

[b] The rate constants of reaction nos. 6 and 19 are in units of s^{-1}; the other rate constants are in units of $l\ mol^{-1}\ s^{-1}$.

[c] The rates of reaction nos. 21–25 and 27–29 are $w_i = k_i\ [Fe^{2+}]\ [\text{bromine-containing compound}]$.

[d] The rate of reaction no. 26 is $w_{26} = (k_{26} + k_{s26}\ [Br^-])[Fe^{3+}][Br^-]$, where $k_{26} = 4 \times 10^{-4}\ l\ mol^{-1}\ s^{-1}$ and $k_{s26} = 1.8 \times 10^{-2}\ l^2\ mol^{-2}\ s^{-1}$.

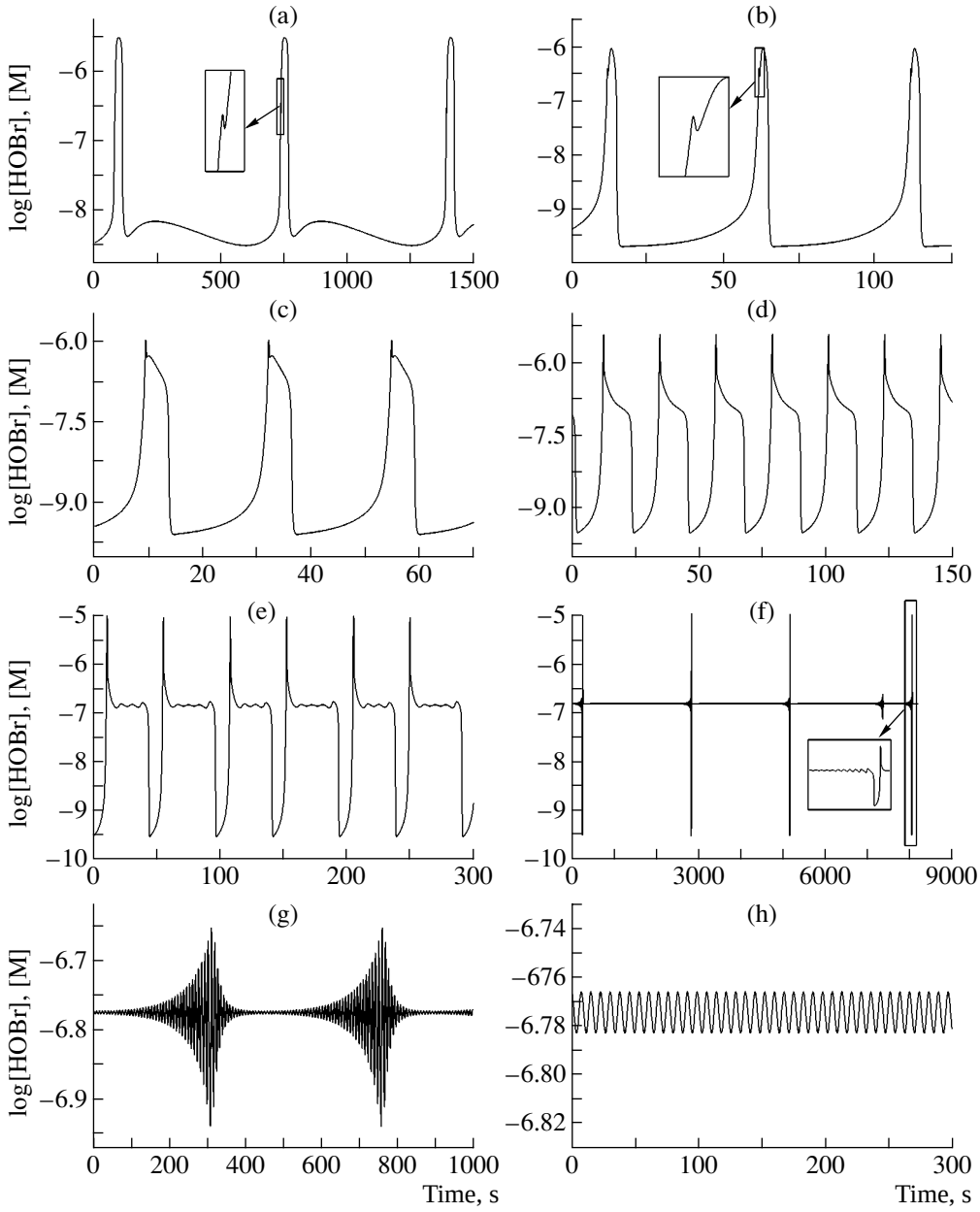

Fig. 3. Time dependence of log[HOBr] obtained by the numerical simulation of the kinetic scheme given in Table 3: (a) LSJ oscillations at $\log k_0$, [s^{-1}] = –4.42, (b) LJ oscillations at $\log k_0$, [s^{-1}] = –3.20, (c) L_1S_1 oscillations at $\log k_0$, [s^{-1}] = –2.25, (d) regular oscillations (R) at $\log k_0$, [s^{-1}] = –1.83, (e) mixed-mode oscillations of the $(L_1S_3)(L_1S_4)$ type at $\log k_0$, [s^{-1}] = –1.66, (f) large-amplitude chaotic oscillations (C_L) at $\log k_0$, [s^{-1}] = –1.55297, (g) quasi-periodic oscillations (QP) at $\log k_0$, [s^{-1}] = –1.55296, and (h) small-amplitude periodic oscillations (ε*R*) at $\log k_0$, [s^{-1}] = –1.55160.

At high values of k_0, chaotic oscillations of the C_L type were observed (Figs. 3f and 4d), which transformed into small-amplitude quasi-periodic QP oscillations (Figs. 3g and 4e) upon a further increase in the flow rate. At $\log k_0$, [s^{-1}] = –1.552933, the system changed to a region of small-amplitude εR oscillations near a steady state, which lost its stability because of a Hopf bifurcation. At $\log k_0$, [s^{-1}] > –1.5515, a sustained steady state was observed in the system (Fig. 4f).

Table 4 summarizes various oscillation regimes for all independent components of the test system; these regimes were obtained at low flow rates. A steady state and a bifurcation region of period doubling are designated by SS and PD, respectively. Oscillations

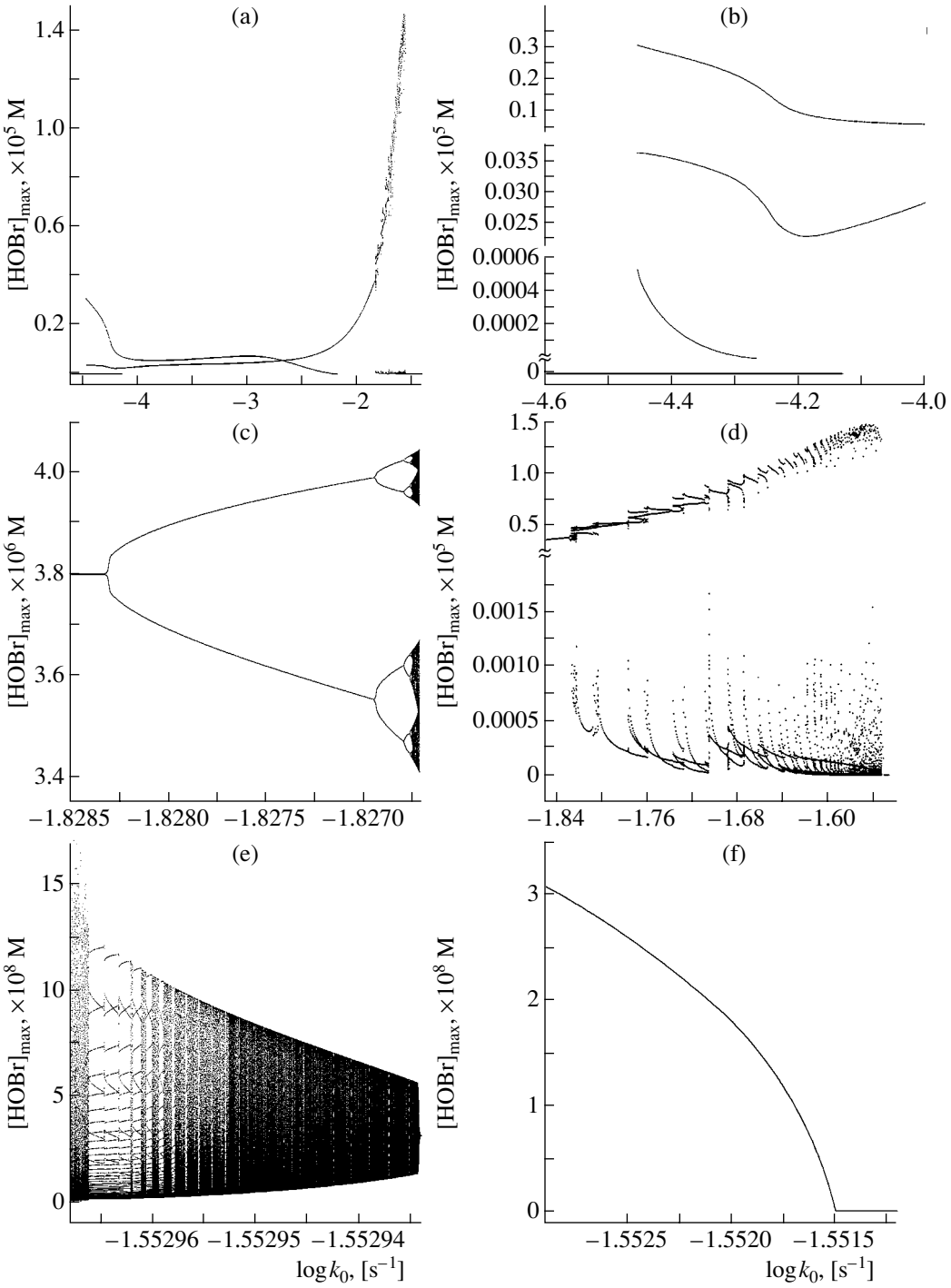

Fig. 4. Bifurcation diagrams of $[HOBr]_{max}$ oscillation amplitudes against $\log k_0$, plotted based on the results of numerical simulation in accordance with the kinetic scheme given in Table 3: (a) bifurcation diagram over the entire range of existence of oscillations, $\log k_0$, $[s^{-1}] = -4.6...-1.4$; (b) bifurcation diagram in the range $\log k_0$ $[s^{-1}] = -4.6...-4.0$, which describes the bifurcation sequence of the appearance of regular (R) oscillations; (c) bifurcation diagram in the range $\log k_0$, $[s^{-1}] = -1.8285\ldots-1.8267$, which describes a period-doubling bifurcation and the appearance of mixed-mode oscillations; (d) bifurcation diagram in the range $\log k_0$, $[s^{-1}] = -1.85\ldots-1.54$, which describes the bifurcations of mixed-mode oscillations; (e) bifurcation diagram in the range $\log k_0$, $[s^{-1}] = -1.552968\ldots-1.552933$, which describes the bifurcations of chaotic C_L and quasi-periodic QP regimes; and (f) bifurcation diagram in the range $\log k_0$, $[s^{-1}] = -1.5528\ldots-1.5512$, which describes a change in oscillation amplitudes near a Hopf bifurcation point.

appeared at the same value of $\log k_0$, [s^{-1}] = –4.456 for all of the BZ reaction components. In the range of $\log k_0$, [s^{-1}] values from –4.456 to –4.130, the coexistence of oscillations and a steady sate was observed. In the bistability region and further up to a value of $\log k_0$, [s^{-1}] equal to –1.8283, system components exhibited regular or mixed-mode L_1S_1 or L_1S_2 oscillations; in this case, the most complex regimes were observed for HOBr and Br_2. In the region $-1.8283 < \log k_0$, [s^{-1}] < –1.8263, a sequence of period-doubling bifurcations occurred. After completion of this sequence, small-amplitude oscillations appeared in the time dependence of HOBr concentration. The positions of these oscillations with respect to a large-amplitude autooscillation are consistent with those found experimentally (see Figs. 1a, 1b, and 3e). Thus, at $\log k_0$, [s^{-1}] > –1.8263, the autooscillations of [HOBr] found by numerical simulation correspond in shape to those found experimentally.

Table 5 summarizes some regimes of [HOBr] oscillations obtained by numerical simulation at flow rates that correspond to the occurrence of mixed-mode oscillations and their disappearance at high k_0. Note that bifurcation sequences are similar for other system components, although the shapes of autooscillations and the amounts of small-amplitude excursions can be different. An analysis of data given in Table 5 demonstrates that an increase in the flow rate is responsible for the appearance of a bifurcation sequence of the addition of small-amplitude excursions, which is qualitatively consistent with the data presented in Table 1. Moreover, in some cases, regimes were observed in which the ratio between small- and large-amplitude oscillations was quantitatively consistent with the experimental data. The occurrence of L_1S_2, $L_1S_3L_1S_4$, $L_1S_4L_1S_5$, L_1S_5, $L_1S_5L_1S_6$, L_1S_7, and L_1S_9 regimes and quasi-periodic oscillations was found both by numerical simulation and experimentally. Note that bifurcations of the L_1S_n regimes were preliminarily observed in the experiments, whereas, according to the numerical simulation, bifurcations of the L_2S_n regimes occurred over a wide range of k_0 ($-1.8025 < \log k_0$, [s^{-1}] < –1.7056). This difference disappeared on going to the region of existence of L_1S_n regimes with $n > 4$. In this case, an increase of k_0 clearly indicates the existence of a bifurcation sequence of the addition of small-amplitude excursions in mixed-mode oscillations (see Table 5). Table 5 gives the regions of

Table 4. Oscillation regimes of reaction components obtained by numerical simulation in accordance with the kinetic scheme (Table 3) at low flow rates (see Table 3 for notations)

$\log k_0$, [s^{-1}]	Autooscillation reaction components											
	Br^-	$HBrO_2$	$BrO_2^{\bullet}$	Fe^{2+}	BrTTA	MA	BrMA	BrO_3^-	$MA^{\bullet}$	$BrMA^{\bullet}$	HOBr	Br_2
–4.456	SS											
–4.392	SS, R	SS, R	SS, R	SS, R	SS, R	SS, R	SS, R	SS, L_1S_1	SS, L_1S_1	SS, R	SS, LSJ	SS, R
–4.304	SS, R	SS, R	SS, R	SS, R	SS, R	SS, R	SS, R	SS, L_1S_1	SS, L_1S_1	SS, R	SS, LSJ	SS, R
–4.296	SS, R	SS, R	SS, R	SS, R	SS, R	SS, R	SS, R	SS, L_1S_1	SS, R	SS, R	SS, LSJ	SS, R
–4.266	SS, R	SS, R	SS, R	SS, R	SS, R	SS, R	SS, R	SS, L_1S_1	SS, R	SS, R	SS, LSJ	SS, LJ
–4.130	SS, R	SS, R	SS, R	SS, R	SS, R	SS, R	SS, R	SS, L_1S_1	SS, R	SS, R	SS, LJ	SS, LJ
–4.090	R	R	R	R	R	R	R	L_1S_1	R	R	LJ	LJ
–3.917	R	R	R	R	R	R	R	R	R	R	LJ	LJ
–3.864	R	R	R	R	R	R	R	R	R	LJ	LJ	LJ
–3.772	R	R	R	R	L_1S_1	R	R	R	R	LJ	L_1S_1	LJ
–3.328	R	R	R	R	R	R	R	R	R	LJ	L_1S_1	LJ
–2.816	R	R	R	R	R	R	R	R	R	LJ	L_1S_1	L_1S_2
–2.756	R	R	R	R	R	L_1S_1	R	R	R	LJ	L_1S_1	L_1S_2
–2.408	R	R	R	R	R	R	R	R	R	LJ	L_1S_1	L_1S_2
–2.340	R	R	R	R	R	R	L_1S_1	R	R	LJ	L_1S_1	L_1S_2
–2.170	R	R	R	R	R	R	R	R	R	LJ	L_1S_1	L_1S_2
–1.8283	R	R	R	R	R	R	R	R	R	LJ	R	L_1S_2
	PD											

Table 5. Some [HOBr] oscillation regimes obtained by numerical simulation in accordance with the kinetic scheme (Table 3) and the ranges of flow rates corresponding to the occurrence of mixed-mode oscillations

Range of $\log(k_0, [s^{-1}])$	Regime
–1.8283···–1.8263	PD
–1.8213···–1.8076	L_3S_1
–1.8025···–1.7770	L_2S_1
–1.7756···–1.7624	$L_2S_1L_2S_2$
–1.7588···–1.7376	L_2S_2
–1.7368···–1.7288	$L_2S_2L_2S_3$
–1.7263···–1.7095	L_2S_3
–1.7088···–1.7056	$L_2S_3L_2S_4$
–1.7044···–1.6900	L_1S_2
–1.6870···–1.6751	L_2S_5
–1.6737···–1.6625	$L_1S_1L_2S_5$
–1.6614···–1.6545	$L_1S_3L_1S_4$
–1.6532···–1.6445	$L_1S_3L_1S_5$
–1.6438···–1.6388	$L_1S_4L_1S_5$
–1.6381···–1.6312	L_1S_5
–1.6306···–1.6282	$L_1S_5L_1S_6$
–1.6268···–1.6213	L_1S_6
–1.6182···–1.6138	L_1S_7
–1.6113···–1.6080	L_1S_8
–1.6057···–1.6028	L_1S_9
–1.6013···–1.5987	L_1S_{10}
–1.5969···–1.5951	L_1S_{11}
–1.5937···–1.5919	L_1S_{12}
–1.5908···–1.5894	L_1S_{13}
–1.552965···–1.552935	QP
–1.552935···–1.5515	εR
>–1.5515	SS

existence of L_1S_n regimes up to the L_1S_{13} regime. At higher k_0, some small-amplitude oscillations degenerated into inflections to result in a formal decrease in the amount of small-amplitude excursions. However, if the numbers of small-amplitude excursions and inflections are taken into account, the regions of existence of L_1S_n mixed modes with $n > 13$ can be found. Data given in Table 5 and Fig. 4d suggest that the widths of the regions of existence of L_1S_n mixed modes decreased with increasing n. Note that, on going from an L_1S_n periodic regime to another one by changing the flow rate, the occurrence of chaotic regimes can be detected at certain k_0. Mixed-mode oscillations and chaotic regimes disappeared at $\log k_0, [s^{-1}] = -1.552965$, and quasi-periodic autooscillations appeared in the system (see Fig. 3g). As k_0 was increased, these oscillations transformed into periodic εR regimes, which occur near a steady state that became unstable because of a Hopf bifurcation. At $\log k_0, [s^{-1}] > -1.5515$, a sustained steady state was observed. Thus, an analysis of data given in Tables 4 and 5 demonstrated that the concentrations of various components in the system can vary in different manners at the same value of k_0; this manifests itself as the occurrence of k_0 ranges with different types of oscillations of component concentrations. However, the bifurcation sequence is common for all system components: SS ⟶ SS, R ⟶ R ⟶ PD ⟶ L_mS_n, and C_L ⟶ QP ⟶ εR ⟶ SS.

Thus, based on an analysis of the kinetic scheme presented in Table 3, we found that the mixed-mode and chaotic oscillations of the ferroin-catalyzed BZ reaction performed in a CSTR can be modeled. We found a qualitative agreement between the experimental and simulated bifurcation sequences and their details observed under changes in the flow rate. As k_0 was increased, bifurcations of the addition of small-amplitude excursions were observed in both experiments and numerical simulation. In the ranges of k_0 values between simple regimes, oscillation sequences consisting of these regimes were observed (see Figs. 1b and 3e). At high flow rates, large-amplitude chaos C_L (see Figs. 1c and 3f and Table 2) and quasi-periodicity QP (see Figs. 1d and 3g) were observed. Based on a comparison between autooscillation regimes observed for various components of the BZ reaction, the commonness of bifurcation sequences for all chemical components of the system was demonstrated. However, we found some differences observed by comparing the results obtained. In particular, L_1S_n regimes were primarily observed in the experiments, whereas the modeling in accordance with the kinetic scheme resulted in L_mS_n regimes over a wide range of k_0. Moreover, we failed to detect J-oscillations in experiments with platinum point, bromide, glass, and carbon electrodes. The kinetic scheme predicts the occurrence of a period-doubling bifurcation and a hysteresis between a steady state and a regular regime, which we failed to detect experimentally because of the narrow region of existence of a period-doubling bifurcation ($\Delta \log k_0, [s^{-1}] \approx 0.002$) and the impossibility of studies at low flow rates.

ACKNOWLEDGMENTS

This work was supported by the grant INTAS-OPEN-97-1094.

APPENDIX

System of differential Eqs. (1) corresponding to the kinetic scheme given in Table 3.

$$\frac{d[Br^-]}{dt} = -k_1[Br^-][BrO_3^-] + k_2[HOBr][HBrO_2]$$
$$-k_3[HBrO_2][Br^-] + k_4[HOBr]^2 - k_5[HOBr][Br^-]$$
$$+k_6[Br_2] + k_{11}[MK][Br_2] + k_{19}[BrTTK]$$
$$+k_{24}[Fe^{2+}][HOBr] + 2k_{25}[Fe^{2+}][Br_2]$$
$$-2(k_{26} + k_{s26}[Br^-])([Fe^{2+}]_0 - [Fe^{2+}])[Br^-]$$
$$+k_0([Br^-]_0 - [Br^-]);$$

$$\frac{d[Br_2]}{dt} = k_5[HOBr][Br^-] - k_6[Br_2]$$
$$-k_{11}[MK][Br_2] - k_{25}[Fe^{2+}][Br_2]$$
$$+(k_{26} + k_{s26}[Br^-])([Fe^{2+}]_0 - [Fe^{2+}])[Br^-] - k_0[Br_2];$$

$$\frac{d[HOBr]}{dt} = k_1[Br^-][BrO_3^-] - k_2[HOBr][HBrO_2]$$
$$+2k_3[HBrO_2][Br^-] - 2k_4[HOBr]^2 - k_5[HOBr][Br^-]$$
$$+k_6[Br_2] + k_7[HBrO_2]^2 - k_8[BrO_3^-][HOBr]$$
$$-k_{12}[MK][HOBr] - k_{13}[BrMK][HOBr]$$
$$+k_{23}[Fe^{2+}][HBrO_2] - k_{24}[Fe^{2+}][HOBr] - k_0[HOBr];$$

$$\frac{d[HBrO_2]}{dt} = k_1[Br^-][BrO_3^-] - k_2[HOBr][HBrO_2]$$
$$-k_3[HBrO_2][Br^-] + k_4[HOBr]^2 - 2k_7[HBrO_2]^2$$
$$+2k_8[BrO_3^-][HOBr] - k_9[BrO_3^-][HBrO_2]$$
$$+k_{10}[BrO_2^\bullet]^2 + k_{15}[BrMK^\bullet][BrO_2^\bullet] + k_{21}[Fe^{2+}][BrO_2^\bullet]$$
$$+k_{22}[Fe^{2+}][BrO_3^-] - k_{23}[Fe^{2+}][HBrO_2] - k_0[HBrO_2];$$

$$\frac{d[BrO_2^\bullet]}{dt} = 2k_9[BrO_3^-][HBrO_2] - 2k_{10}[BrO_2^\bullet]^2$$
$$-k_{15}[BrMK^\bullet][BrO_2^\bullet] - k_{17}[MK^\bullet][BrO_2^\bullet]$$
$$+k_{18}[MK^\bullet][BrO_3^-] + k_{20}[BrMK^\bullet][BrO_3^-]$$
$$-k_{21}[Fe^{2+}][BrO_2^\bullet] - k_0[BrO_2^\bullet];$$

$$\frac{d[BrO_3^-]}{dt} = -k_1[Br^-][BrO_3^-] + k_2[HOBr][HBrO_2]$$
$$+k_7[HBrO_2]^2 - k_8[BrO_3^-][HOBr]$$
$$-k_9[BrO_3^-][HBrO_2] + k_{10}[BrO_2^\bullet]^2$$
$$-k_{18}[MK^\bullet][BrO_3^-] - k_{20}[BrMK^\bullet][BrO_3^-]$$
$$-k_{22}[Fe^{2+}][BrO_3^-] + k_0([BrO_3^-]_0 - [BrO_3^-]);$$

$$\frac{d[BrTTK]}{dt} = k_{14}[BrMK^\bullet]^2 + k_{15}[BrMK^\bullet][BrO_2^\bullet]$$
$$+k_{16}[BrMK^\bullet][MK^\bullet] - k_{19}[BrTTK]$$
$$+k_{20}[BrMK^\bullet][BrO_3^-] - k_0[BrTTK];$$

$$\frac{d[MK]}{dt} = -k_{11}[MK][Br_2] - k_{12}[MK][HOBr]$$
$$+k_{16}[BrMK^\bullet][MK^\bullet] - k_{27}([Fe^{2+}]_0 - [Fe^{2+}])[MK]$$
$$+k_0([MK]_0 - MK);$$

$$\frac{d[MK^\bullet]}{dt} = -k_{16}[BrMK^\bullet][MK^\bullet]$$
$$-k_{17}[MK^\bullet][BrO_2^\bullet] - k_{18}[MK^\bullet][BrO_3^-]$$
$$+k_{27}([Fe^{2+}]_0 - [Fe^{2+}])[MK] - k_0[MK^\bullet];$$

$$\frac{d[BrMK]}{dt} = k_{11}[MK][Br_2] + k_{12}[MK][HOBr]$$
$$-k_{13}[BrMK][HOBr] + k_{14}[BrMK^\bullet]^2$$
$$-k_{28}([Fe^{2+}]_0 - [Fe^{2+}])[BrMK]$$
$$+k_{29}[Fe^{2+}][BrMK^\bullet] - k_0[BrMK];$$

$$\frac{d[BrMK^\bullet]}{dt} = -2k_{14}[BrMK^\bullet]^2 - k_{15}[BrMK^\bullet][BrO_2^\bullet]$$
$$-k_{16}[BrMK^\bullet][MK^\bullet] - k_{20}[BrMK^\bullet][BrO_3^-]$$
$$+k_{28}([Fe^{2+}]_0 - [Fe^{2+}])[BrMK]$$
$$-k_{29}[Fe^{2+}][BrMK^\bullet] - k_0[BrMK^\bullet];$$

$$\frac{d[Fe^{2+}]}{dt} = -k_{21}[Fe^{2+}][BrO_2^\bullet] - 2[Fe^{2+}]$$
$$\times(k_{22}[BrO_3^-] + k_{23}[HBrO_2] + k_{24}[HOBr] + k_{25}[Br_2])$$
$$+2(k_{26} + k_{s26}[Br^-])([Fe^{2+}]_0 - [Fe^{2+}])[Br^-]$$
$$+k_{27}([Fe^{2+}]_0 - [Fe^{2+}])[MK]$$
$$+k_{28}([Fe^{2+}]_0 - [Fe^{2+}])[BrMK]$$
$$-k_{29}[Fe^{2+}][BrMK^\bullet] + k_0([Fe^{2+}]_0 - [Fe^{2+}]).$$

REFERENCES

1. *Oscillations and Travelling Waves in Chemical Systems*, Field, R. and Burger, M., Eds., New-York: Wiley, 1985.
2. Epstein, I.R., *Physica D*, 1983, vol. 7, p. 47.
3. Schneider, F.W. and Münster, A.F., *J. Chem. Phys.*, 1991, vol. 95, no. 6, p. 2130.
4. Zhabotinsky, A.M., *Chaos*, 1991, vol. 1, no. 4, p. 379.
5. Epstein, I.R. and Showalter, K.C., *J. Phys. Chem.*, 1996, vol. 100, no. 31, p. 13132.
6. Hudson, J.L., Hart, M., and Marinko, D., *J. Chem. Phys.*, 1979, vol. 71, no. 4, p. 1601.
7. Argoul, F., Arneodo, A., Richetti, P., and Roux, J.C., *J. Chem. Phys.*, 1987, vol. 86, no. 6, p. 3325.
8. Richetti, P., Roux, J.-C., Argoul, F., and Arneodo, A., *J. Chem. Phys.*, 1987, vol. 86, no. 6, p. 3339.
9. Barkley, D., *J. Chem. Phys.*, 1988, vol. 89, no. 9, p. 5547.
10. Györgyi, L., Turanyi, T., and Field, R.J., *J. Phys. Chem.*, 1990, vol. 94, no. 18, p. 7162.
11. Györgyi, L. and Field, R.J., *J. Phys. Chem.*, 1991, vol. 95, no. 17, p. 6594.
12. Noskov, O.V., Karavaev, A.D., Spivak, S.I., and Kazakov, V.P., *Kinet. Katal.*, 1992, vol. 33, no. 3, p. 704.
13. Zhabotinsky, A.M., Buchholtz, F., Kiyatkin, A.B., and Epstein, I.R., *J. Phys. Chem.*, 1993, vol. 97, no. 29, p. 7578.
14. Strizhak, P.E. and Kawczynski, A.L., *J. Phys. Chem.*, 1995, vol. 99, no. 27, p. 10830.
15. Goryachev, A., Strizhak, P., and Kapral, R., *J. Chem. Phys.*, 1997, vol. 107, no. 8, p. 2881.
16. Taylor, A.F., Johnson, B.R., and Scott, S.K., *J. Chem. Soc., Faraday Trans.*, 1998, vol. 94, no. 8, p. 1029.
17. Dolnik, M., Rovinsky, A.B., Zhabotinsky, A.M., and Epstein, I.R., *J. Phys. Chem., A*, 1999, vol. 103, no. 1, p. 38.
18. Noszticzius, Z., McCormick, W.D., and Swinney, H.L., *J. Phys. Chem.*, 1987, vol. 91, no. 19, p. 5119.
19. Yatsimirskii, K.B., Strizhak, P.E., and Ivashchenko, T.S., *Talanta*, 1993, vol. 40, no. 8, p. 1227.
20. Buravlev, E.P., Sirenko, L.A., Strizhak, P.E., and Smirnova, N.N., *Fiziol. Rast.*, 1994, vol. 41, no. 2, p. 299.
21. Rovinsky, A.B. and Zhabotinsky, A.M., *J. Phys. Chem.*, 1984, vol. 88, no. 25, p. 6081.
22. Keki, S., Magyar, I., Beck, M.T., and Gaspar, V., *J. Phys. Chem.*, 1992, vol. 96, no. 4, p. 1725.
23. Strizhak, P.E., Khavrus', V.A., Goncharenko, M.M., and Ivashchenko, T.S., *Teor. Eksp. Khim.*, 1998, vol. 34, no. 3, p. 153.
24. Wolf, A., Swift, J.B., Swinney, H.L., and Vastano, J.A., *Physica D*, 1985, vol. 16, nos. 1–3, p. 285.
25. Hindmarsh, A.C., *Technical Report No. UCID-3001*, Livermore: Lawrence Livermore Laboratory, 1972.